Direct microwave heating of alumina for different densities: experimental and numerical thermal analysis

Inès Ghorbel, Patrick Ganster, Nicolas Moulin, Christophe Meunier, Julien Bruchon

Direct microwave heating of Alumina at different densities: Numerical and experimental thermal analysis

Inès Ghorbel, Patrick Ganster, Nicolas Moulin, Christophe Meunier, Julien Bruchon

Mines Saint-Etienne, Univ. Lyon, CNRS, UMR 5307 LGF, Centre SMS, F - 42023 Saint-Etienne France

Abstract

Microwave heating of pure alumina is studied experimentally and numerically, in a 2.45 GHz single-mode cavity, for different density levels. Even considering a constant incident power, the results show a complex evolution of the alumina temperature: first an increase in two steps, then a maximum and finally a cooling stage. In addition, a density dependence of the heating efficiency is observed: a better heating occurs for lower densities. Using the Effective Medium Approximation (EMA) to derive the physical data as functions of density, the numerical simulations are in contradiction with the experiments, proving that the EMA approach is not able to correctly predict the imaginary part of the permittivity. Furthermore, the simulations do not accurately describe the first moments of the heating, nor the long-term evolution of the temperature (cooling). We then explain the origin of this discrepancy: the need to adjust the movable stub on the one hand, and to account for heat exchange between the cavity and its surroundings on the other.

Highlights

- Experimental and numerical study of alumina microwave heating
- Effective medium approximation
- Impact of sample density on the microwave heating

Key words: Microwave heating, Alumina, permittivity, Effective Medium Approximation, relative density, Modelling

Email addresses: ines.ghorbel@emse.fr (Inès Ghorbel), ganster@emse.fr (Patrick Ganster), nmoulin@emse.fr (Nicolas Moulin), meunier@emse.fr (Christophe Meunier), bruchon@emse.fr (Julien Bruchon)

1. Introduction

The study of ceramic by microwave heating has been developed considerably over the last decade, in parallel with the modelling of the process [17, 4, 12, 9, 11, 14, 13, 6, 7]. Despite these advances, the process is difficult to control and the modelling requires physical parameters that are mostly unavailable. Thus, it is necessary to use predictive models and/or approximations to derive these parameters.

Indeed, during sintering, the properties of the material change throughout the thermal cycle, natably due to the evolution of its microstructure. For a material such as alumina, which shows a weak coupling to the microwaves, susceptors (made of a material such as Silicon Carbide, which couples strongly to microwaves) are usually placed near the sample to facilitate heating at low temperature until coupling starts at higher temperatures.

This paper aims to highlight the effect of density on microwave heating of pure alumina. Direct microwave heating is therefore realised using 2.45 GHz monomode cavity and the associated modeling is carried out using COMSOL Multiphysics© software [1]. The p̂hysical parameters are derived using the effective medium approximation [17].

2. Material and methods: experimental setup

Two sets of samples were prepared with a high purity alumina powder [3] using conventional heating. First, cylinders are prepared to perform dilatometric tests during a sintering cycle, and hence to establish evolution of the density with temperature. Second, parallelepipedal samples of different densities are prepared to study microwave heating. Here, the density refers to a perfectly densified sample of alpha-alumina (reference value: ρ_{th} = 3.987 g.cm^{-3}).

2.1. Dilatometric tests

Dilatometric tests measure the shrinkage of the sample during sintering and evaluate the corresponding density during a thermal cycle. A Setaram dilatometer (Setsys 16/18) is used. Figure 1 shows the working principle of this dilatometer, used in a conventional oven. The sample is placed on an alumina support and an alumina feeler is brought into contact with the top surface of the sample. During a controlled thermal cycle, the feeler follows the height of the sample, thus characterising the deformation of the sample. This includes shrinkage due to sintering and the thermal dilatation of the sample. The temperature is measured using a type B thermocouple (T max =1700°C) positioned under the sample. The dilatometric tests are preceded by a blank recording which allows the thermal dilatation of the entire equipment (feeler and support) to be eliminated from the measurements.

The dilatometric tests are performed on cylindrical samples of 8 mm diameter. The samples are shaped by compacting the alumina powder into a cylindrical matrix with an uni-axial press, applying a pressure of 100 MPa. Prior to the dilatometric measurements, a debinding thermal cycle was applied to the samples in order to eliminate the organic elements binding the powder. This cycle consists of increasing the temperature at 1°C/min, up to 600°C. This plateau is then maintained for 60 minutes, before cooling at 1°C/min.

The dilatometric tests are carried out with the following thermal cycle: a temperature increase at 5°C / min, a dwell time of 5 min at 1600 °C followed by a cooling at 20°C / min. As only the height of the sample is measured during this cycle, the change in the relative density is obtained

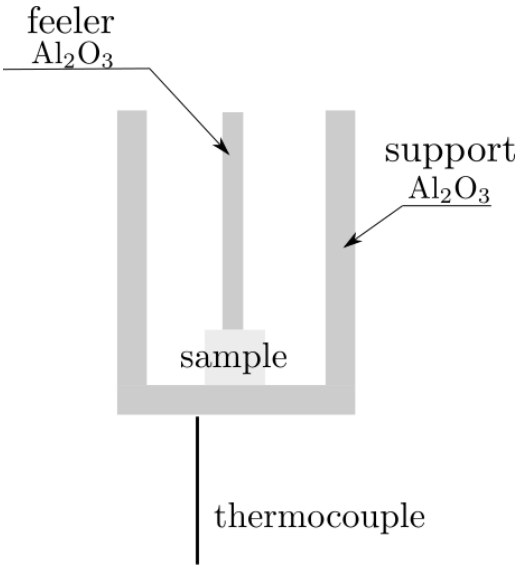

Figure 1: Working principle of the dilatometer.

from the anisotropic coefficient defined by evaluating the density before and after the thermal cycle [10]. This coefficient α is defined as:

$$\alpha = \frac{d_f - d_0}{d_0} \times \frac{h_f - h_0}{h_0} \tag{1}$$

where d_0, d_f are the initial and the final diameters, h_0 and h_f are the initial and the final heights.

From the measured height $h(t)$ of the sample, the relative density $D(t)$ writes [10]:

$$D(t) = \frac{\left(1 + \frac{h_f - h_0}{h_0}\right) \times \left(1 + \frac{d_f - d_0}{d_0}\right)^2}{\left(1 + \frac{h(t) - h_0}{h_0}\right) \times \left(1 + \alpha \times \frac{h(t) - h_0}{h_0}\right)^2} \times \frac{\overline{\rho}_f}{\overline{\rho}_{th}} \tag{2}$$

where $\overline{\rho}_f$ is the final density. The density $D(t)$ is plotted in Figure 2, as a function of temperature during the applied thermal cycle. It is shown that the sintering starts at 1373 K (1100°C), while the relative density increases from 43.8% to 97%.

To investigate the density dependence of microwave heating, parallelepipedal samples with relative densities of 43.8% (green sample), 55% and 97% respectively were prepared. They are first shaped by compacting 5.28 g of alumina powder into a parallelepipedic matrix of size 25×9.1 mm^2 using a uniaxial press and with a pressure of 50 MPa. The thermal cycles are subsequently applied in a conventional oven:

- For the samples with a density of 55%, the thermal cycle consists of a heating at 5°C/min, until reaching 1200 °C, allowed by a cooling at room temperature.
- For the samples with a density of 97%s, the thermal cycle consists of a heating at 5°C/min, until reaching 1600°C, a dwell time of 2 hours and a cooling at 5°C/min.

Each sample is then rectified to the same dimensions of 9.5 mm × 7.5 mm × 19 mm to avoid the size effects during microwave heating.

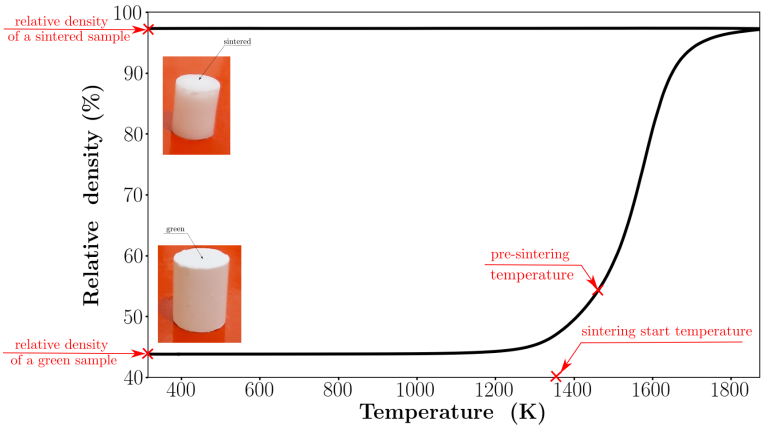

Figure 2: Relative density of an alumina sample, plotted as a function of temperature during a thermal cycle.

3. Microwave setup

3.1. Experimental setup and calibration

A 2.45 GHz single-mode microwave setup, illustrated in Figure 3, is used to study the microwave heating of the alumina samples. It is composed of: a solid state microwave generator

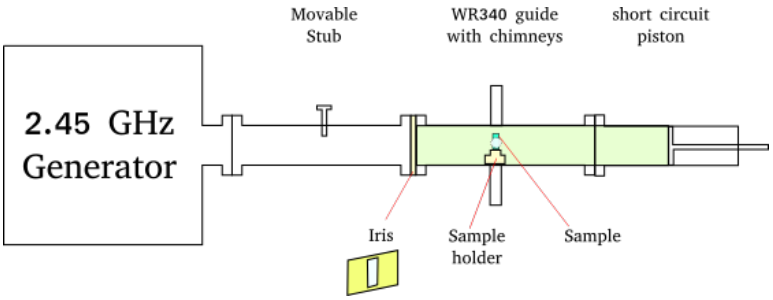

Figure 3: Schematic design of the 2.45 GHz single-mode microwave device.

(Sairem GMSP10) delivering a continuous wave with a power up to 900 W, at frequencies ranging from 2.4 GHz to 2.5 GHz [18]; a movable stub; a rectangular cavity delimited on one side by a 15x43 mm rectangular iris, on the other side by a short-circuit piston allowing to adjust the length of the cavity; a WR 340 waveguide with three cylindrical chimneys disposed at the maxima of the electric field (for an empty cavity).

In our experiments, the sample is placed on a thermally insulating support[1], a fibrous alumina-silicate material composed of 80% alumina and 20% silica. In the field of ceramic sintering, this material is often chosen because it meets all the criteria imposed by the use of high-temperature microwave radiation: low thermal conductivity, good resistance to thermal shock and a high melting point allowing temperatures up to 1800°C. The geometry of the support corresponds to

[1] Altraform ® from RATH company [16]

that described in reference [9]. In addition, the samples are oriented in such a way that the heating is as efficient as possible: its largest dimension is aligned with the electric field polarisation.

Before any microwave heating experiment, the length of the cavity must be adjusted to the resonance length, in order to obtain a stationary electric field of maximum magnitude. This tuning is performed only at room temperature, for the cavity in which the sample and the insulating support are placed. The temperature dependence of the resonance length is not considered in this work in order to limit the number of variables and to facilitate the comparison with simulations. To find the optimal length of the cavity, considering an incident power of 50 W, the cavity length is adjusted to minimise the reflected power. Then, and only after sufficient time without applying microwaves, the heating experiment can begin. Our experiments consist in applying a constant microwave power and measuring the temperature of the sample with a pyrometer operating at 2.4 μm. The pyrometer was calibrated by determining the apparent emissivity of the alumina samples for the three different densities, in a conventional oven under black body conditions. More precisely, the sample is placed in a hollow alumina cylinder whose height is more than four times greater than its inner diameter. For different temperature steps, the apparent emissivity of the device is adjusted to recover, with the pyrometer, the temperature measured by a thermocouple.

The apparent emissivity of the three categories of alumina samples is plotted as a function of temperature in Figure 4, for a temperature range [373 K - 1173 K]. The results show that

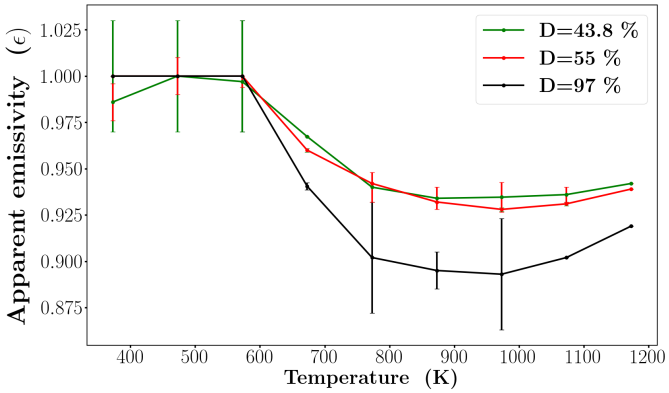

Figure 4: Apparent emissivity of alumina samples with relative densities of 43.8%, 55% and 97%, in the temperature range [373 K - 1173 K].

the apparent emissivity corresponding to the device calibration does not depend on the alumina density in the whole temperature range. The alumina emissivity is between 0.8 and 0.95 as defined by the pyrometer manufacturer for ceramic materials.

3.2. Numerical setup

The COMSOL multiphysics software is used for modelling the microwave heating of alumina with the different relative densities. The 3D geometry of the cavity is given in Figure 5 (from reference [9]), as well as the boundary conditions of the thermal problem (à détailler un peu plus ou modifier la figure. The single-mode cavity is excited with a TE_{104} electric field at 2.45 GHz.

As in our previous work describing the heating of Silicon Carbide (SiC) [9], and in order to compare the numerical results with experiments, the computational domain, where the electro-

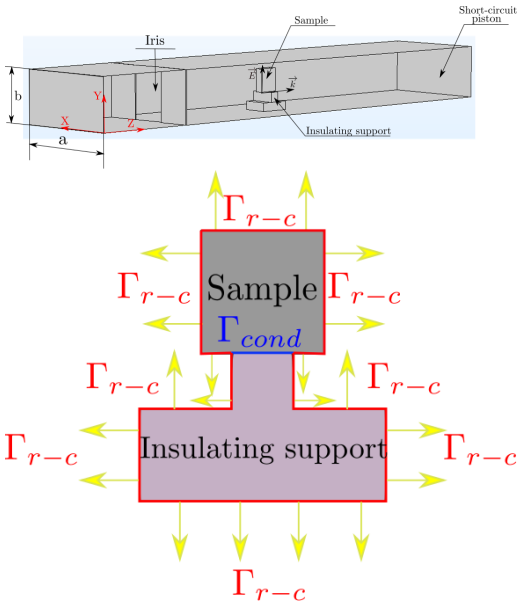

Figure 5: Top: geometry of the single-mode cavity. Bottom: Boundary conditions of the thermal problem used for Alumina microwave heating [9].

magnetic and thermal equations are solved, is reduced and simplified. This domain consists of the cavity delimited by an iris and a short-circuit piston, which contains the sample placed on the insulating support as described in Figure 5. The generator and movable stub are not described in order to limit the computational cost. Details of the solved equations and numerical validations can be found in reference [9].

Although the dielectric [14] and thermal [2] properties of alumina can be found in literature as functions of temperature, their dependence on the density is unfortunately unknown. In this work, the effective medium approximation (EMA) [5, 13] is considered to derive this density dependence of the different physical parameters of alumina involved in the numerical model. In addition, the thermal insulating support is not considered to be transparent to microwaves, as its dielectric properties are close to those of the alumina samples. Indeed, the material of the insulating support is composed of a porous Al_2O_3 / SiO_2 mixture. The thermal and dielectric properties of the insulating support are obtained from the work of Manière et *al.* [13, 12]. All the expressions of the physical properties of the materials used are given in the supplementary notes. Table 1 shows the ranges of these different parameters at the different densities for a temperature between 300 K and 1500 K.

These parameters are the input data for the simulations. More precisely, using the geometry described in Figure 5, the length of the cavity (in which an alumina sample and the insulating support are placed) is first adjusted to the resonance length, using a constant incident power of 50 W and minimising the reflected power, exactly as in the experimental protocol (as this determination is carried out at room temperature, only one resolution of the electromagnetic problem is required). Once the resonance length is found, a constant incident power is applied, and electromagnetic and thermal equations are solved alternatively (weak coupling), in the whole computational domain (cavity, support and sample) for the former, only support and sample for

Table 1: Physical parameters of alumina (real and imaginary parts of the permittivity, ε' and ε'', heat capacity at constant pressure C_p, thermal conductivity κ) obtained by EMA for three different densities (D=43.8%, D=55%, D=97%) in the range of temperature [300 K - 1500 K].

	D= 43.8 %	D= 55 %	D= 97 %
ε'	3-3.8	4.08-4.6	8.3-9.9
ε''	6×10^{-4} - 8×10^{-3}	1.5×10^{-3} - 1.9×10^{-2}	4.7×10^{-3} - 0.057
C_p (J.kg^{-1}.K^{-1})	343-573	431-720	761.5-1270
κ (W.m^{-1}.K^{-1})	5.8-0.9	12-1.9	35-5.6

the thermal part [9]. The same thermal cycles as in the experiments are considered. The results of the experiments and simulations are presented in the next section.

4. Results

4.1. Experimental results

The dependence of microwave heating on density was studied by considering two incident powers of 50 W and 100 W respectively. Figure 6(a) shows, for these two powers, the temperature changes as a function of time obtained when considering a sample of density 55%. The corresponding reflected power is plotted in Figure 6(b). With the 50 W power, the temperature evolution is characterised by a first fast increase in the initial moments of the heating, followed by a slowdown to a dwell-like temperature at 100 s. Then, a second fast temperature increase is observed until a maximum is reached, before the sample slowly cools down. This maximum temperature is of 440±5 K, reached in the interval [t = 250 s, t = 500 s]. The reflected power is correlated to this temperature evolution and more particularly to the heating rate. It first increases to a maximum which corresponds to the slowdown of the temperature increase. Then, the reflected power decreases to a minimum during the second fast temperature increase. Finally, the reflected power increases again following a monotonous behaviour that corresponds to the achievement of a maximum temperature and the slow cooling of the sample.

With the 100 W power, a faster and higher heating is produced and the same trend is observed on the evolution of the reflected power. The maximum temperature is also reached in two stages: even if the first stage is too short to be detected by looking at the temperature evolution, it presence is confirmed by the behaviour of the reflected power. If we now compare the two temperature curves obtained with the 50 W and 100 W powers, we can observe that no significant temperature gain is obtained when the power supplied is doubled: the maximum temperature is 442 K at 400 s for 50 W, compared with 467 K at 175 s for 100 W. This is consistent with the dielectric properties of alumina, which is a material with a low coupling to the electric field. This point is highlighted by the value of the reflected power: the final reflected power ranges from 1% to 20% of the incident power when heating a SiC sample [9], but increases to 40-50% in the case of alumina.

The temperature evolution of samples with relative densities of 43.8%, 55% and 97%, and the corresponding reflected power, for an incident power of 50 W and 100 W, are given Figures 7(a)-(d). For the 50 W power (Figure 7(a)), the maximum temperatures are 480 K, 440 K and 325 K for samples with relative density of 43.8%, 55% and 97% respectively. Note that most of the time, the temperature of the 97% density sample is lower than the minimum temperature that

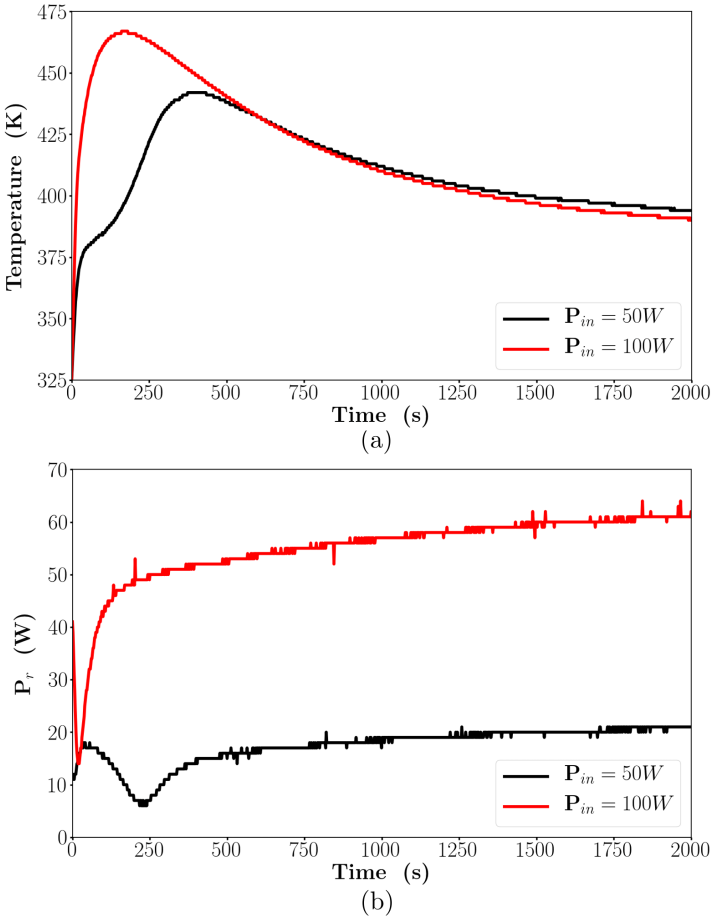

Figure 6: (a) Temperature evolution of an alumina sample with a density of 55%, for incidents powers of 50 W and 100 W respectively, and (b) corresponding reflected power.

the pyrometer can detect, which gives rise to the peaks observed on the graph. The behaviour of temperature and reflected power (Figure 7(c)) is similar to the description given above, except for the 97% density. Indeed, the reflected power evolution is different, with a monotonous behaviour and a significantly higher final value. It also appears that the maximum temperature is reached at a shorter time compared to the other densities.

Figures 7(b) and 7(d) show the results for an incident power of 100 W power: higher temperatures are reached in shorter times. The maximum temperature reached is 540 K, 467 K and 445 K for 43.8%, 55% and 97% samples, respectively. In each case, the reflected power increases at the beginning to reach a first maximum, then decreases to a minimum, before increasing monotonously until the end of the experiment. These overall results clearly show that the heating is dependent on the density of the alumina. The lower the density, the higher the microwave heating efficiency. The complex evolution of the sample temperature, correlated with the reflected power, will be discussed in the discussion section.

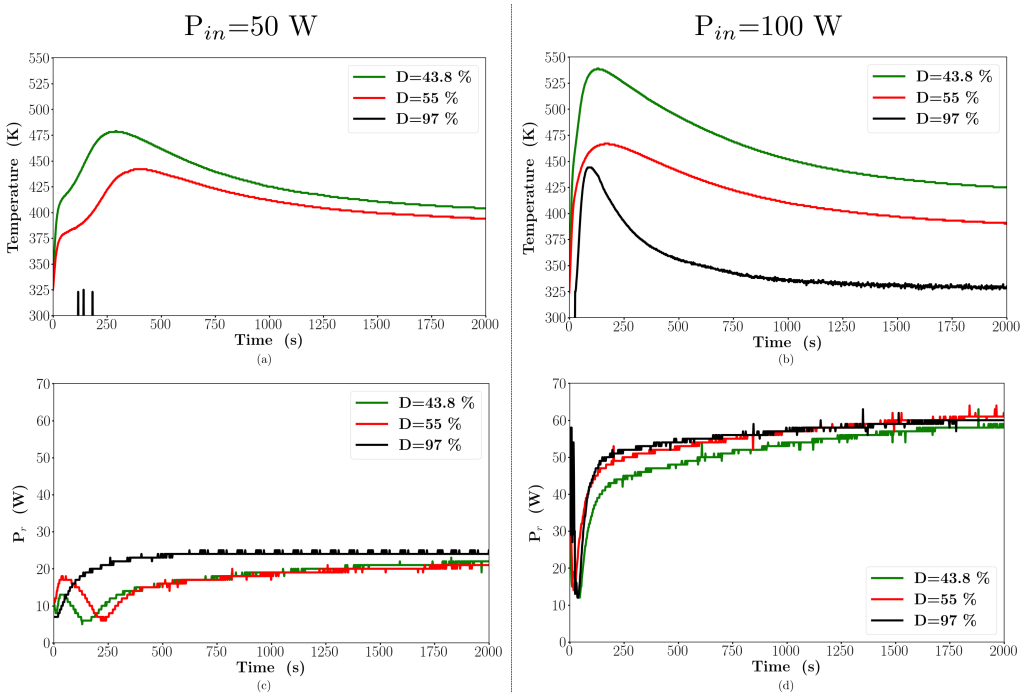

Figure 7: Evolution of temperature and reflected power during microwave heating, for incident powers of 50 W (left) and 100 W (right) and alumina samples with relative densities of 43.8%, 55% and 97%.

4.2. Numerical results

As already mentioned, the resonance length of the cavity is determined before any heating simulation. Figure 8 shows the intensity of the electric field intensity averaged over the alumina sample, obtained for different cavity lengths and for the three densities (D=43.8%, D=55% and D=97%). The length corresponding to the maximum intensity is also the resonant length: 337.6 mm, 336.7 mm and 334.3 mm for D=43.8%, D=55% and D=97% respectively. The resonance lengths found by the simulation are smaller than those obtained experimentally (star markers in Figure 8), which are 344 mm, 343 mm and 341 mm for D=43.8%, D=55% and D=97% respectively. The density dependence is however respected since the denser the sample, the shorter the cavity lengthy. The observed differences are certainly due to the assumptions made in the simulations: simplification of the geometry (no description of the chimney) and cavity walls considered as perfect electrical conductors.

The heating of samples with different densities is simulated using an incident power of 50 W, a fixed cavity length and the physical parameters provided by EMA approximation and given in Table 1. Figure 9 presents the evolution of the simulated temperature at the sample surface for the three relative densities. For each density, the temperature first increases monotonously, until reaching a steady state. The maximum temperature is then 320 K at 260s, 350 K at 500s and 395 K at 2000s for the D=43.8%, D=55% and D=97% respectively. These results are significantly different from the experimental observations. Indeed, the two-step temperature increase is not observed, an inverse order in the density dependence of the heating efficiency is obtained, and the longer term temperature decrease is not described. This discrepancy between the experi-

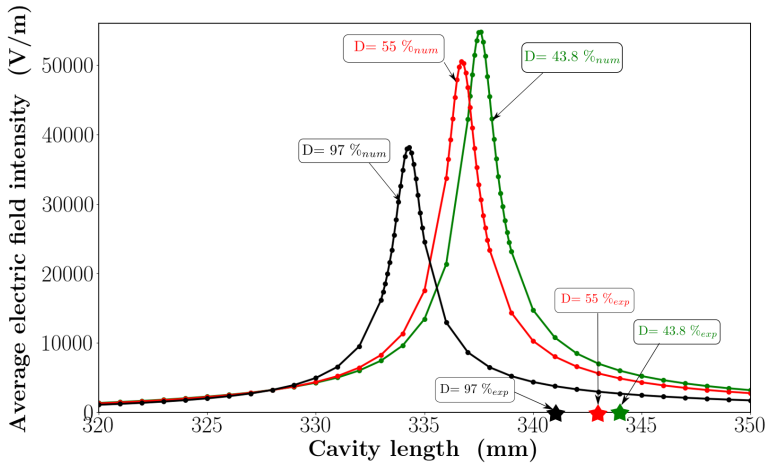

Figure 8: Average intensity of the electric field obtained by simulation for different cavity lengths and the three densities (D=43.8%, D=55% and D=97%). Star markers correspond to the resonant cavity lengths measured experimentally.

mental and simulation results is discussed in the next discussion section.

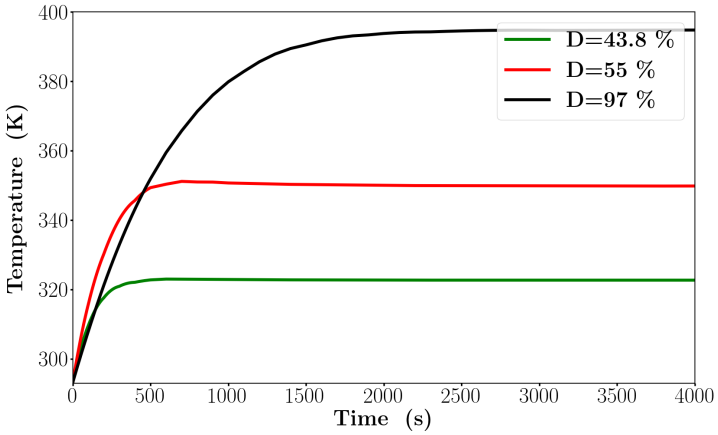

Figure 9: Evolution of the temperature during the microwave heating of an alumina sample, for the three densities (43.8%, 55% and 97%), obtained by numerical simulation using EMA approximation.

5. Discussion

5.1. EMA approximation

The most remarkable difference between the simulation and the experimental results concerns the density dependence of the heating efficiency: the most efficient heating is obtained for D = 43.8% experimentally, and D = 97% numerically. This is because the EMA approximation is unable to describe the experimental imaginary part of the permittivity of porous alumina. Table 2 provides a comparison at room temperature, of the complex permittivity found in the

literature, for porous and sintered alumina, either from experimental measurements [8, 15], or predicted by the EMA approximation. The values of ε' found by the EMA approximation are in agreement with the experimental results of Gershon *et al.* [8] and Penn *et al.* [15] for both porous and sintered samples. However, the imaginary part of the permittivity ε'' provided by the EMA

Table 2: Measured and predicted complex permittivity of porous and sintered alumina at ambient temperature.

	ε'	ε''
EMA (D= 55%)	4.05	0.0012
Measured (Submicron sized D= 55.5% [8])	3.99	0.029
Measured (Micron sized D= 59.3% [8])	4.33	0.018
EMA (D= 97%)	8.36	0.004
Measured (Submicron sized D= 97.5 % [8])	8.82	0.0003
Measured (Micron sized D= 96.8% [8])	9.22	0.004
Measured (sintered polycrystalline alumina [15])	10	-

approach is in the contradiction with the experimental results [8, 15]. The imaginary part of the permittivity should increase when the density decreases.

Simulations using the imaginary part of the permittivity deduced from experimental data were then performed. Gershon's values [8] being limited to the densities D=55% and D=97%, we deduced values from the work of Penn *et al.* [15] who measured and successfully modelled the real part of the permittivity ε' and the loss factor $\tan\delta$ as functions of the porosity:

$$\varepsilon' = \varepsilon_m \left(1 - \frac{3(1-D)(\varepsilon_m - 1)}{2\varepsilon_m + 1}\right) \tag{3}$$

and

$$\tan\delta = D\ \tan\delta_0 + A'(1-D)\left(\frac{1-D}{D}\right)^{2/3} \tag{4}$$

where D is the relative density, $\varepsilon_m = 10$ at ambient temperature for dense alumina material, $\tan\delta_0 = 1.565 \times 10^{-5}$ and $A' = 9.277 \times 10^{-3}$.

Using Equations (3)-(4), and $\tan\delta = \frac{\varepsilon''}{\varepsilon'} = \frac{\varepsilon''_r}{\varepsilon'_r}$, the new values of ε'' calculated for the three relative densities are presented in Table 3.

Table 3: New values of the imaginary part of the permittivity of alumina.

	D = 43.8%	D = 55%	D = 97%
ε''	0.017	0.015	0.0004

The previous simulations are now carried out using these new values of ε''. The cavity resonant lengths are not affected by this change. The microwave heating is then simulated for the three densities, considering constant values of the dielectric parameters (*i.e.* without temperature dependence), whereas the thermal parameters (C_p and κ) depend on the temperature (see Appendix **??** and Table 1). Figure 10 shows the temperature evolution during the microwave heating for the three relative densities and using the new values of ε''. The most efficient heating is obtained with the lowest density D = 43.8%, followed by the intermediate one D = 55%.

For D = 97%, the sample does not heat up: a temperature increase of only 0.2 K is observed. These results are in agreement with the experiences where the more porous sample, the more efficient heating. The complex experimental temperature evolution in two steps is however not obtained.The results also show that the steady temperature is reached in a shorter time for D = 43.8%. This is in agreement with the experimental measurements: the lower the specific heat C_p, the faster the maximum temperature is reached.

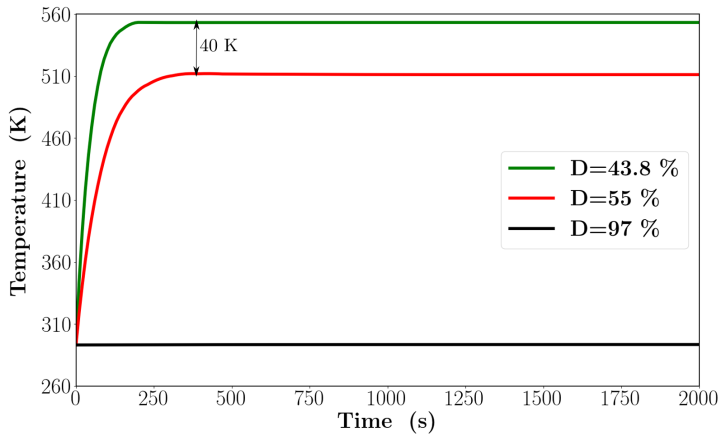

Figure 10: Evolution of the temperature during microwave heating for D = 43.8%, D = 55% and D = 97%, using the new values of ε'' provided in Table 3.

5.2. Initial heating stages

As shown above, the two-step heating is not captured by the simulations, which do not take the movable stub into account, in order to limit the computational time and resources. The movable stub is used to adapt the impedance of the full cavity system, and thus to optimise the stationary conditions at the resonance. However, in all previous experiments, the stub has the same position and is kept fixed during heating. The influence of the stub on the heating is now investigated experimentally using a Vector Network Analyser (VNA) to optimise its position and depth, and the short circuit piston to find the best resonance length at 2.45 GHz for a 55% relative density sample. Figure 11 shows the evolution of the temperature and the corresponding reflected power in two cases: when the resonance conditions are optimised by the position and depth of the stub and the length of the cavity ("Tuned" curves); when the position and depth of the stub are not optimal ("Disrupted" curves).

When the stub is optimally adjusted, the temperature increases in one step: a maximum is reached before cooling. In this case, the corresponding reflected power is negligible at the initial stage and then increases monotonously. In a disrupted position, the heating occurs in two steps as observed in the first experiments. In this case, the reflected power first decreases (over the time interval [100s, 250s]) until the system becomes fully resonant (because of the heating and the temperature dependence of the resonance length). Due to the increase in temperature, this resonant state is lost, the reflected power increases (t > 250 s) causing the the sample to cool. This result highlights the importance of the position and depth of movable stub, and explains why the simulation fails to describe the initial stages of the experimental heating.

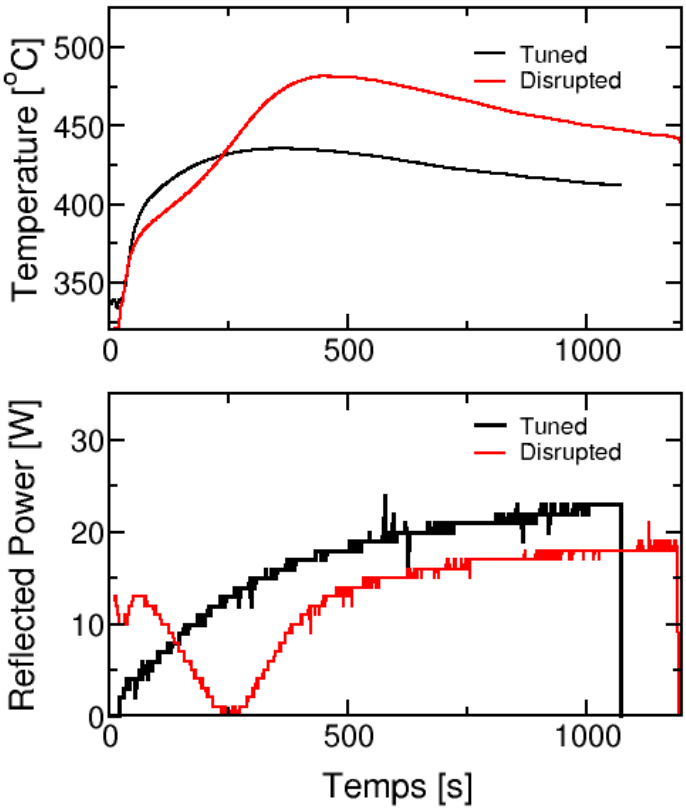

Figure 11: Evolution of (a) temperature and (b) reflected power, during the microwave heating of a 55% relative density alumina when both the movable stub and the cavity length are optimally tuned ("Tuned" curves), and when the stub is not well adjusted ("Disrupted" curves).

5.3. long heating times

The cooling observed over longer times is also not captured by the simulations. This behaviour may result from complex heat transfers and/or microwave couplings between the sample and the insulating support. To examine this assumption, we performed two experiments using a sample made of insulating support material (RATH®) with the same dimensions as the previous alumina samples. This ensures the same physical properties of the sample and the support. The first heating experiment is conducted under the same conditions as before, *i.e.* without cooling the cavity. In contrast, the second heating experiment is carried out in a cavity placed in an environment in which the air is cooled. For both experiments, an incident power of 100 W power is considered. Using a VNA, the cavity resonance at 2.45 GHz is first achieved by adjusting the movable stub and the short circuit piston.

Figure 12 presents the evolution of the temperature and reflected power during these experiments. In the first moments of both experiments, the two step-heating is no longer observed because the system is properly tuned. Consequently, the corresponding reflected power does not fluctuate and increases monotonously. The insulating support and the sample, made of the same

material, heat up uniformly. After the sample has reached a maximum temperature, the same cooling behaviour as for an alumina sample is observed. The temperature decrease is greater when the cavity is in a room temperature environment than when the environment is cooled.

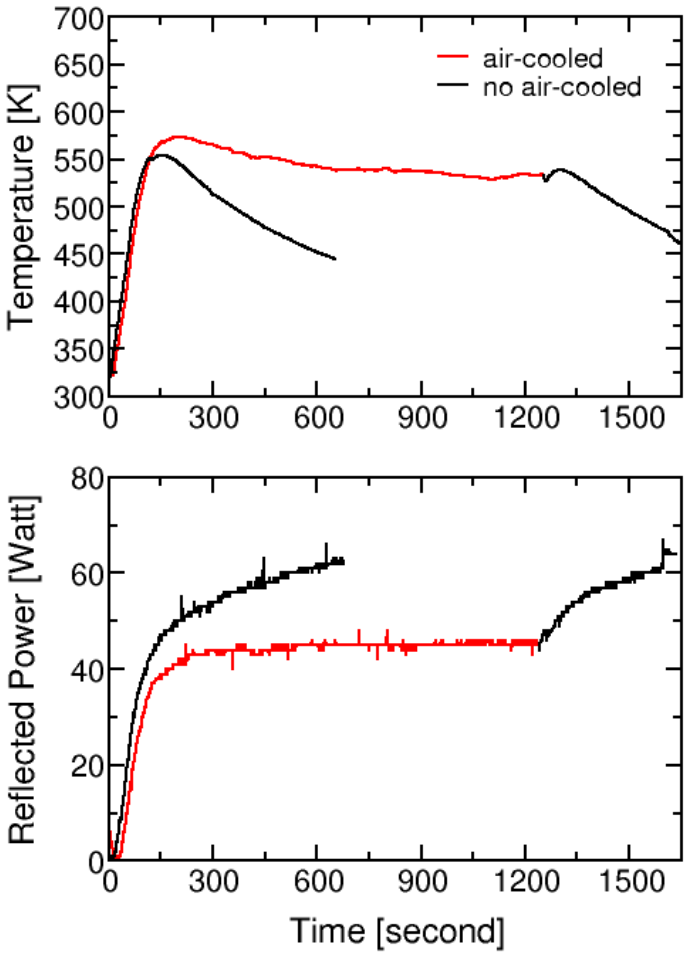

Figure 12: Evolution of (a) temperature and (b) reflected power during microwave heating of a RATH® sample, with and without air cooling.

In the air-cooling experiment, we observe a fast decrease in the sample temperature and a corresponding increase in reflected power after the cooling system is switched off at 1250 s. This phenomenon clearly indicates that, over long heating times, the cavity temperature has a huge influence on the sample temperature. It can be noted that this effect is not observed in the case of microwave heating of SiC, as SiC is good absorber material. For low absorber materials as alumina or silica-alumina, a significant part of the electromagnetic energy is dissipated in the cavity walls, which are heated, thus detuning the resonant system. This effect degrades the efficiency of the sample heating. This also explains why the simulations presented in this paper

do not reproduce the long-term heating of alumina, whereas they describe the heating of SiC accurately [9].

6. Conclusion

The microwave heating of parallelepipedal alumina samples of three different densities (D = 43.8%, D = 55% and D = 97%) in a 2.45 GHz single-mode cavity, was studied experimentally and numerically. After adjusting the cavity length for each sample to the resonant length at room temperature, the alumina samples were heated using a constant incident power of 50 W or 100 W. The results show a complex evolution of the sample temperature: first, a temperature increase in two steps, then a maximum, and finally a cooling stage. It is also observed that the lower the density of the sample, the higher the heating efficiency.

To analyse the experimental results, simulations with COMSOL multiphysics© were performed. The density dependence of the physical parameters of alumina was derived from the Effective Medium Approximation. The numerical results appeared to be in contradiction with the experimental results, showing that the EMA approach is unable to predict the imaginary part of the permittivity of alumina, which decreases with increasing densities. The experimental trend was however found by the simulations when using data from experimental permittivity measurements. However, the simulations are still far from the experimental results for the early stages of heating and long-term heating. Further experiments were conducted to explain these differences.

First, the influence of the movable stub, which was not taken into account in the simulations, was evaluated. It appeared that an appropriate adjustment of the stub makes the two-step temperature increase disappear. Regarding the long-term heating behaviour, the experiments showed that the insulating support was not responsible for cooling the sample. They highlighted the role of the cavity wall temperature and the heat exchange of the cavity with its surroundings: when the cavity is placed in an environment where the air is cooled, the temperature of the sample decreases at a much lower rate. Finally, it has to be pointed out that all these phenomena occur because alumina and silica-alumina are low absorber materials. These results show that a complete and accurate numerical description of microwave heating of this type of materials require taking into account the "details" of the cavity geometry, as well as extending the thermal problem (limited in this work to the sample-support system) to the whole cavity.

A. Material properties

Table A.1: Electromagnetic-thermal material properties [13, 12, 14].

Material	Symbol (unit)	Temperature range (K)	Expression
Insulation	C_p (J.kg^{-1}.K^{-1})	273-1200 K	5.82×10^{2}+1.25T-$5.31\times10^{-4}T^{2}$
	κ (W.m^{-1}.K^{-1})	273-1200 K	6.15×10^{-2}+ 1.74×10^{-4}T
	$\overline{\rho}$ (kg.m^{-3})	273-1200 K	4.43×10^{2}-1.04×10^{-2}T
	ϵ	273-1200 K	0.83
	ε_r	273-1200 K	1. (microwave transparent)
SiC	C_p (J.kg^{-1}.K^{-1})	273-673 K	-8.35+3.08T-$0.00293T^{2}$+$1.0268\times10^{-6}T^{3}$
		673-1200 K	772+0.431T-$2.1\times10^{-5}T^{2}$
	κ (W.m^{-1}.K^{-1})	273-1200 K	192-0.326T+$2.74\times10^{-4}T^{2}$-$7.71\times10^{-8}T^{3}$
	$\overline{\rho}$ (kg.m^{-3})	273-1200 K	2977+0.051T-$2.29\times10^{-4}T^{2}$+$2.98\times10^{-7}T^{3}$ -$1.92\times10^{-10}T^{4}$+$4.77\times10^{-14}T^{5}$
	ϵ	273-1200 K	-$1.239\times10^{-12}T^{4}$+$4.51\times10^{-9}T^{3}$-$6.1142\times10^{-6}T^{2}$ +0.0037T+0.1436
	$\varepsilon_r^{'}$	273-1200 K	6.4-1.67×10^{-3}T+$1.88\times10^{-6}T^{2}$
	$\varepsilon_r^{''}$	273-1200 K	0.992-3.43×10^{-4}T+$7.72\times10^{-6}T^{2}$-$7.15\times 10^{-9}T^{3}$ +$2.36\times10^{-12}T^{4}$
Air	C_p (J.kg^{-1}.K^{-1})	273-1200 K	961+0.177T
	κ (W.m^{-1}.K^{-1})	273-1200 K	0.0035+6×10^{-5}T
	$\overline{\rho}$ (kg.m^{-3})	273-1200 K	0.02897P/(RT)
	ε_r	273-1200 K	1

References

[1] Comsol multiphysics®. https://www.comsol.com.

[2] Al_2O_3. Alumina thermal parameters:. http://www-ferp.ucsd.edu/LIB/PROPS/PANOS/al2o3.html.

[3] A. Borrell and M. D. Salvador. Baikowski®society : url=https ://www.baikowski.com/fr/.

[4] A. Borrell and M. D. Salvador. Advanced ceramic materials sintered by microwave technology. In M. Liu, editor, *Sintering Technology*, chapter 1. IntechOpen, Rijeka, 2018.

[5] Y. V. Bykov, K. I. Rybakov, and V. E. Semenov. High-temperature microwave processing of materials. *Journal of Physics D: Applied Physics*, 34(13):R55, 2001.

[6] J. Croquesel, D. Bouvard, J.-M. Chaix, C. P. Carry, and S. Saunier. Development of an instrumented and automated single mode cavity for ceramic microwave sintering: Application to an alpha pure alumina powder. *Materials & Design*, 88:98 – 105, 2015.

[7] T. Garnault, D. Bouvard, J.-M. Chaix, S. Marinel, and C. Harnois. Is direct microwave heating well suited for sintering ceramics? *Ceramics International*, 47(12):16716–16729, 2021.

[8] D. Gershon, J. Calame, and A. Birnboim. Complex permittivity measurements and mixing laws of porous alumina. *Journal of Applied Physics*, 89, 06 2001.

[9] I. Ghorbel, P. Ganster, N. Moulin, C. Meunier, and J. Bruchon. Experimental and numerical thermal analysis for direct microwave heating of silicon carbide. *Journal of the American Ceramic Society*, 104(1):302–312, 2021.

[10] D. Lance, F. Valdivieso, and P. Goeuriot. Correlation between densification rate and microstructural evolution for pure alpha alumina. *Journal of the European Ceramic Society*, 24(9):2749 – 2761, 2004.

[11] C. Manière, S. Chan, and E. A. Olevsky. Microwave sintering of complex shapes: From multiphysics simulation to improvements of process scalability. *Journal of the American Ceramic Society*, 102(2):611–620, 2019.

[12] C. Manière, L. Geuntak, T. Zahrah, and E. A. Olevsky. Microwave flash sintering of metal powders: From experimental evidence to multiphysics simulation. *Acta Materialia*, 147:24 – 34, 2018.

[13] C. Manière, T. Zahrah, and E. A. Olevsky. Fully coupled electro-magnetic-thermal-mechanical comparative simulation of direct vs hybrid microwave sintering of 3Y-ZrO2. *Journal of the American Ceramic Society*, 100(6):2439–2450, 2016.

[14] S. Marinel, C. Manière, A. Bilot, C. Bilot, C. Harnois, G. Riquet, F. Valdivieso, C. Meunier, C. Coureau, and F. Barthélemy. Microwave sintering of alumina at 915 MHz: Modeling, process control, and microstructure distribution. *Materials*, 12:2544, 08 2019.

[15] S. J. Penn, N. M. Alford, A. Templeton, X. Wang, M. Xu, M. Reece, and K. Schrapel. Effect of porosity and grain size on the microwave dielectric properties of sintered alumina. *Journal of the American Ceramic Society*, 80(7):1885–1888, 1997.

[16] Rath. ©rath-group:. https://www.rath-group.com/en/products/insulating-fire-bricks.

[17] K. I. Rybakov, E. A. Olevsky, and E. V. Krikun. Microwave sintering: Fundamentals and modeling. *Journal of the American Ceramic Society*, 96:1003–1020, March 2013 2013.

[18] SAIREM. SAIREM documentation. https://www.sairem.com/wp-content/uploads/2019/02/GMSP10-EN.pdf.